# UC Irvine
## UC Irvine Previously Published Works

**Title**

Ex vivo validation of photo-magnetic imaging.

**Permalink**

**Journal**

**ISSN**

**Authors**

Luk, Alex
Nouizi, Farouk
Erkol, Hakan
et al.

**Publication Date**

**DOI**

Peer reviewed

# *Ex vivo* validation of photo-magnetic imaging

**Alex Luk**[1], **Farouk Nouizi**[1,*], **Hakan Erkol**[1], **Mehmet B. Unlu**[3], **Gultekin Gulsen**[1,2]

[1]Tu and Yuen Center for Functional Onco-Imaging, Department of Radiological Sciences, University of California, Irvine, California 92697, USA

[2]Department of Biomedical Engineering, University of California, Irvine, California 92697, USA

[3]Department of Physics, Bogazici University, Bebek, Istanbul, Turkey

## Abstract

We recently introduced a new high-resolution diffuse optical imaging technique termed photo-magnetic imaging (PMI), which utilizes magnetic resonance thermometry (MRT) to monitor the 3D temperature distribution induced in a medium illuminated with a near-infrared light. The spatiotemporal temperature distribution due to light absorption can be accurately estimated using a combined photon propagation and heat diffusion model. High-resolution optical absorption images are then obtained by iteratively minimizing the error between the measured and modeled temperature distributions. We have previously demonstrated the feasibility of PMI with experimental studies using tissue simulating agarose phantoms. In this Letter, we present the preliminary *ex vivo* PMI results obtained with a chicken breast sample. Similarly to the results obtained on phantoms, the reconstructed images reveal that PMI can quantitatively resolve an inclusion with a 3 mm diameter embedded deep in a biological tissue sample with only 10% error. These encouraging results demonstrate the high performance of PMI in *ex vivo* biological tissue and its potential for *in vivo* imaging.

Diffuse optical tomography (DOT) is an imaging modality that aims to recover the optical absorption of tissue from multiple measurements performed on its boundary by solving a nonlinear inverse problem [1]. Despite its high sensitivity, DOT provides very poor spatial resolution due to the highly scattering nature of biological tissue, which drastically decreases the penetration depth of photons [2]. Moreover, light sources and detectors placed on the tissue boundary allow only the performance of surface measurements making the inverse problem strongly under-determined and ill posed yielding non-unique solutions [3]. During the resolution of the inverse problem of DOT, a sensitivity matrix is implemented. This matrix describes the changes in measurements due to small variations in the internal optical properties. Following that, this matrix needs to be inverted, generally using unstable pseudo-

*Corresponding author: fnouizi@uci.edu.

inversion techniques [4]. In fact, the sensitivity matrix is not square because the number of measurements is much smaller than the number of unknowns to be reconstructed [5]. It has been shown that performing internal measurements reduces the under-determination of the inverse problem and makes the inversion of the sensitivity matrix more stable [6].

We have previously introduced photo-magnetic imaging (PMI), a novel approach for diffuse optical imaging that is capable of performing internal measurements [6,7]. The boundary measurements performed on the surface in conventional optical imaging are not very sensitive to the variation of contrast deep in tissue. Our new approach not only increases the number of measurements but more importantly acquires them within the whole volume, thus considerably increasing its sensitivity. PMI leverages magnetic resonance thermometry (MRT) to measure the time-dependent temperature variations induced by the absorption of near-infrared light [8]. This allows PMI to perform internal measurements unlike the conventional photon fluence detection at the boundaries of the imaged medium. Using a hybrid model combining photon propagation and heat diffusion, the forward problem of PMI generates synthetic spatiotemporal temperature variations in a turbid medium illuminated using light at a particular wavelength. The diffusion equation is widely used to model the light propagation within highly scattering media [9,10]. Considering the optical absorption of the medium, the photon's energy is converted to heat [11] and used as a source term in the bio-heat equation to generate spatiotemporal temperature maps [12]. This system of combined equations is usually solved using either the finite element method (FEM) [6,7] or analytical methods [13–16]. As a final step, these simulated temperature maps are compared to the measured ones obtained by MRT to solve the PMI inverse problem and obtain high-resolution optical absorption maps. We previously demonstrated the superior performance of PMI with extensive phantom studies simulating biological tissue [6]. In this Letter, we present the first *ex vivo* experimental results obtained on a chicken breast sample.

The spatiotemporal temperature map within the medium is obtained by solving the PMI forward problem defined by the following diffusion and the Pennes bio-heat transfer equations [6,7,11,17]:

$$\begin{cases} -\nabla D(r) \nabla \Phi(r) + \mu_a(r) \Phi(r) = S(r) \\ \rho c \dfrac{\partial T(r,t)}{\partial t} - \nabla k \nabla T(r,t) = \Phi(r)\mu_a(r) \end{cases} \tag{1}$$

where $\mu_a[\text{mm}^{-1}]$ is the absorption coefficient; $D$ is the diffusion coefficient, $D(r) = 1/[3(\mu_a + \mu'_s)]$; $\mu'_s[\text{mm}^{-1}]$ is the reduced scattering coefficient; $\Phi(r)[\text{W} \cdot \text{mm}^{-2}]$ is the photon density at position $r$ [mm]; and $S(r)$ is the isotropic light source. For the heat equation, $\rho$ is the density [g mm$^{-3}$], $c$ is the specific heat [J(g°C)$^{-1}$], and $k$ is the thermal conductivity [W(mm°C)$^{-1}$] of the medium. The source of thermal energy induced by the laser is defined as the product of the optical absorption and the photon density at any point within the medium as expressed by the right-hand side of the bio-heat equation in Eq. (1) [7]. While performing *ex vivo* studies, the metabolic heating and blood perfusion terms are neglected in the heat equation. The Neumann [18] and the heat convection boundary conditions are utilized for the diffusion and bio-heat equations, respectively.

During the resolution of the inverse problem, the absorption coefficient update $\mu_a$ is obtained by [6]

$$\Delta \mu_a = (J^T J + \lambda I) J^T (T^M - F(\mu_{a-ini})), \tag{2}$$

where $J$ is the sensitivity matrix, and $T^M$ is the high-resolution measured MRT temperature map. The FEM forward operator $F$ generates the simulated spatiotemporal temperatures using the initial spatial distribution of the absorption coefficient $\mu_{a-ini}$. Here, $\lambda$ is the regularization parameter and $I$ is the identity matrix.

The experiments are performed using a commercial breast coil designed for a Philips Achieva 3T MR scanner. The medium under investigation is placed inside the coil and illuminated from both sides. A high-power (808 nm, 7 W) fiber coupled laser (Focuslight, China) is utilized to heat the sample. The output of the laser is transferred to the sample positioned at the center of the breast coil via two 15 m long optical fibers. Light is collimated at the output of the fibers using Newport Optics aspherical lenses to provide uniform illumination with a spot diameter of 15 mm. The laser power, after the collimator, is measured with a power meter and adjusted to 0.31 W/cm$^2$. This exposure level is under the maximum permissible exposure (MPE) at 808 nm for an illumination of 10 s, which is defined by the American National Standards Institute (0.32 W/cm$^2$).

The laser-induced temperature variation is measured by MRT using the proton resonance frequency shift method [8]. Figure 1(b) shows the dynamic MRT acquisition timeline consisting of multiple frames with a temporal resolution of 8 s. First, the laser position in the axial direction is precisely located using a T1-weighted image using a fiducial marker. Following this, the dynamic MRT acquisition is initiated and the first phase map is acquired and used as a baseline prior to turning the laser on. Afterward, the laser is turned on at the beginning of the second frame to warm up the medium under investigation and the dynamic MRT measurements are acquired for the following frames. The laser-induced temperature variation based on the phase shift between any frame and the baseline is calculated during the postprocessing step [11]. The resulting temperature variation map is utilized during the PMI image reconstruction, Eq. (2). In fact, each pixel of this image is used as an independent temperature measurement for the reconstruction algorithm [6]. The high spatial resolution of the MRT images constitutes a large number of measurements, which are distributed internally within the whole medium, yielding the reduction of the ill-posed PMI inverse problem and obtaining high-resolution optical absorption images that are quantitatively accurate [6].

Prior to performing *ex vivo* studies, our high-resolution PMI technique is evaluated using a complex phantom with multiple inclusions. The complex phantom consists of a 25 mm cylindrical agarose phantom bearing nine 2 mm diameter cylindrical inclusions positioned in a 3 × 3 matrix separated by 1 mm from each other, Fig. 2(a). The absorption and scattering of the background are set to 0.013 mm$^{-1}$ and 0.8 mm$^{-1}$, respectively, by adjusting the amounts of India ink and intralipid in the agar solution. The inclusions are made by filling predrilled holes with a different agar solution that has a two times higher absorption coefficient, 0.026 mm$^{-1}$. For this phantom study, the thermal properties are set to be the

same as water with the thermal conductivity, $k$, set to $0.6 \times 10^{-3}$ W(mm°C)$^{-1}$, and the density and specific heat of the phantom are set to 1000 kg m$^{-3}$ and 4200(J kg°C)$^{-1}$, respectively. The measurements are obtained using a gradient echo sequence with a repetition time (TR) and echo time (TE), which are 107 ms and 24 ms, respectively. The field of view (FOV) and the slice-thickness are set to 60 mm × 60 mm and 5 mm, respectively, while the MRT image pixel size is 0.23 mm × 0.23 mm. The MRT phase map is acquired during the heating cycle between 8 and 16 s, Fig. 1(b). As previously mentioned, this phase map is used in the postprocessing step to generate a temperature map that describes the increase in temperature during this period [6]. The more pronounced temperature rise is observed close to the surface under the illumination sites and also within the nine inclusions. Although all nine inclusions have the same optical absorption contrast, the observed temperature increase is different for each inclusion and strongly depends on the distance from the light sources as can be seen in Fig. 2(b). This effect can clearly be seen in the profiles performed on the temperature map along lines AB and CD, Figs. 2(d) and 2(e), respectively. Nevertheless, all nine inclusions can be directly localized in this temperature map prior to any reconstruction process.

Our dedicated PMI reconstruction algorithm is utilized to recover the high-resolution absorption map using this measured temperature distribution, Fig. 2(c). Figure 2(c) shows that all nine inclusions are resolved successfully and their absorption value is recovered with high quantitative accuracy. Slight reconstruction artifacts are noticed on this map. Nevertheless, their maximum error value is around only 5% of the absorption of the inclusions so that these artifacts can be negligible. These artifacts result from the mismatch in the estimation of the laser power and the initial optical and thermal properties [6]. The profiles carried out on the reconstructed absorption map along the lines AB and CD [Figs. 2(d) and 2(e), respectively] show the ability of PMI to resolve these closely seated inclusions. First, the size of the inclusions is estimated from the full width at half-maximum (FWHM) of these profiles. The estimated diameters from the profiles range between 1.75 mm and 1.95 mm. The mean error in the recovered size is 9.4% while the maximum error is 12.5%. Accurately resolving the size of the inclusions allows the PMI to recover their absorption coefficient with high accuracy. The maximum error in the recovered absorption coefficient is 9.6%. The error for most of the inclusions is less than 6% when the peak absorption value in the reconstructed object is considered. Following these phantom results, a chicken breast sample is utilized to verify the *ex vivo* performance of PMI. Chicken breast is widely used as the *ex vivo* validation sample due to its unknown optical and thermal properties as well as its slightly heterogeneous composition. The dimensions of this chicken breast sample are 82 mm $x$ × 30 mm $y$ × 45 mm $z$. A 3.5 mm hole is drilled along the $z$-axis and filled with an agarose mixture to mimic a high-absorbing heterogeneity. The absorption and scattering of this mixture are set to 0.041 mm$^{-1}$ and 0.8 mm$^{-1}$, respectively. In order to enhance the contrast of the inclusion in the T1-weighted MR image, a 0.2% solution containing Gadolinium (Omniscan, USA), is added to this mixture, Fig. 3(a). The MRT measurements are acquired using a gradient echo sequence with TR/TE = 55/24 ms, FOV = 120 mm × 120 mm, MR image pixel size = 0.47 mm × 0.47 mm, and slice – thickness = 3 mm. Although the drilled hole has a circular shape, an elliptical cross section is observed in the MR image due to the elasticity of chicken breast tissue, which distorts the shape of the

hole, Fig. 3(a). In this experiment, the chicken breast sample is illuminated from only two sides as shown by the red arrows, Fig. 3(a). The temperature profiles carried out across the inclusion between the illumination direction (CD) and its orthogonal direction (AB) are depicted in Figs. 3(c) and 3(d), respectively. The profile (CD) shows the high increase in temperature under the illumination sites. As expected, the temperature decreases as the photons propagate deeper in the tissue away from its surface. Nevertheless, a substantial increase in temperature is observed at the inclusion even though it is positioned nearly 13 mm under the closest surface. This is uniquely due to the high optical absorption of the inclusion compared to the background [6]. Prior to solving the PMI inverse problem, the initial background absorption coefficient of the chicken breast tissue sample needs to be determined. For this purpose, the MRT temperature measurements are utilized. However, to eliminate the influence of the inclusion, only the temperature measurements up to 5 mm deep on both illumination sites are used. First, based on values reported in the literature, the scattering parameter is set to 0.2 mm$^{-1}$ [19] and the thermal properties are chosen to be those of the chicken breast with 75% water content and 0.6% fat [20]. Then, the difference between the measured MRT and the FEM simulated temperature distributions under the illumination area is minimized in order to estimate the absorption value, which will later be used to initialize the reconstruction algorithm. The optical absorption value obtained using this step is 0.0097 mm$^{-1}$, which is in good agreement with the results reported in the literature [19]. Finally, using these optical and thermal properties, the FEM-based PMI image reconstruction problem is initialized then solved to generate a high-resolution optical absorption map [6,7].

The FEM mesh is generated using the boundary of the sample delineated on the anatomical T1-weighted MR image. Figure 3(b) shows the reconstructed high-resolution absorption map demonstrating the high performance of PMI in resolving the inclusion buried 13 mm deep in the chicken breast sample.

The maximum and mean values of absorption are 0.045 mm$^{-1}$ and 0.0384 mm$^{-1}$, respectively. When the maximum and mean absorption values are considered, the errors in the recovered absorption value of the inclusion are 9.8% and 6.3%, respectively. However, the reconstructed map shows some slight reconstruction artifacts under the illumination sites certainly due to the mismatch of the optical and thermal properties with our chicken breast sample, since we set the scattering coefficient to a value from literature in the algorithm. In addition, a slightly larger artifact is observed to the left of the inclusion. This artifact is due to the small leak of the agar mixture to a void area created during the drilling of the hole. Nevertheless, these artifacts can be negligible as their maximum error value represents less than 7% of the maximum absorption recovered in the inclusion. The profiles across the inclusion along AB and CD show the high quantification accuracy of our technique, Figs. 3(c) and 3(d). The size of the inclusion measured from the MR anatomic image is 4.28 mm and 2.91 mm in AB (*x*-axis) and CD (*y*-axis), respectively. PMI reconstructed an inclusion of size 4.22 mm in the *x*- and 3.2 mm in the *y*-directions. This represents a slight error of 2% and 9% in the *x*- and *y*-directions, respectively.

Please notice that unlike DOT, illuminating the sample from only two sides does not degrade the PMI spatial resolution and the inclusion sizes are well recovered in both *x*- and *y*-

directions. These experiments demonstrate not only the high performance of our PMI technique but also its superior spatial resolution and high quantitative accuracy. The phantom studies show that PMI can recover objects as small as 2 mm located deep within a complex turbid medium. It would be impossible to resolve these closely seated small objects in a turbid medium with conventional diffuse optical imaging techniques since utilizing only surface measurements yields images with poor spatial resolution due to the ill-posedness of their inverse problem. On the other hand, the recently emerged new photoacoustic imaging technique is also able to provide such high spatial resolution images. However, its major disadvantage is the depth dependence of its spatial resolution. Since PMI acquires internal measurements from the whole volume, it provides exceptional spatial resolution compared to conventional optical imaging modalities. In fact, PMI is able to maintain its high performance as long as the variation of temperature is above the sensitivity of MRT (0.1 °C). In addition, using only continuous wave lasers, it can be a low-cost add-on to any MRI system. In the future, with the implementation of multiple wavelengths, PMI can provide the same functional information provided by conventional optical imaging techniques, namely, water, fat, and oxy- and deoxy-hemoglobin maps as well as distribution of exogenous contrast agents. These high-resolution and quantitatively accurate concentration maps of chromophores and contrast agents will be useful for many applications such as cancer imaging and characterization. The preliminary *ex vivo* PMI results presented in this Letter are the first step in translating this novel technology to the preclinical and clinical area. The results have shown that the PMI can probe several centimeters deep in tissue. In addition to that, the *ex vivo* experiments also allowed us to test the robustness of the PMI image reconstruction algorithm under more heterogeneous and unknown optical and thermal properties than those of homogeneous agarose phantoms prepared in our laboratory. It is an important step that will be critical for *in vivo* imaging. After these successful *ex vivo* results, our next step will be implementing a multi-wavelength approach and applying PMI for *in vivo* small-animal imaging.

## Acknowledgments

## REFERENCES

1. Gibson A, Hebden J, and Arridge SR, Phys. Med. Biol 50, R1 (2005). [PubMed: 15773619]

2. Hebden J, Arridge S, and Delpy D, Phys. Med. Biol 42, 825 (1997). [PubMed: 9172262]

3. Arridge SR and Lionheart WRB, Opt. Lett 23, 882 (1998). [PubMed: 18087373]

4. Yalavarthy PK, Pogue BW, Dehghani H, and Paulsen KD, Med. Phys 34, 2085 (2007). [PubMed: 17654912]

5. Arridge SR, Inverse Probl 15, R41 (1999).

6. Nouizi F, Luk A, Thayer D, Lin Y, Ha S, and Gulsen G, J. Biomed. Opt 21, 16009 (2016). [PubMed: 26790644]

7. Lin Y, Gao H, Thayer D, Luk A, and Gulsen G, Phys. Med. Biol 58, 3551 (2013). [PubMed: 23640084]

8. Rieke V and Butts Pauly K., J. Magn. Reson. Imaging 27, 376 (2008). [PubMed: 18219673]

9. Schweiger M, Arridge SR, Hiraoka M, and Delpy DT, Med. Phys 22, 1779 (1995). [PubMed: 8587533]

10. Dehghani H, Srinivasan S, Pogue BW, and Gibson A, Philos. Trans. R. Soc. A 367, 3073 (2009).

11. Thayer DA, Lin Y, Luk A, and Gulsen G, Appl. Phys. Lett 101, 83703 (2012). [PubMed: 22991481]

12. Wissler EH, J. Appl. Physiol 85, 35 (1985).

13. Nouizi F, Erkol H, Luk A, Unlu MB, and Gulsen G, Biomed. Opt. Express 7, 3899 (2016). [PubMed: 27867701]

14. Erkol H, Nouizi F, Luk A, Unlu MB, and Gulsen G, Opt. Express 23, 31069 (2015). [PubMed: 26698736]

15. Alqasemi U, Salehi HS, and Zhu Q, J. Opt. Soc. Am. A 33, 205 (2016).

16. Erkol H, Nouizi F, Unlu MB, and Gulsen G, Phys. Med. Biol 60, 5103 (2015). [PubMed: 26083326]

17. Nouizi F, Erkol H, Luk A, Marks M, Unlu MB, and Gulsen G, Phys. Med. Biol 61, 7448 (2016). [PubMed: 27694717]

18. Nouizi F, Chabrier R, Torregrossa M, and Poulet P, Proc. SPIE 7369, 73690C (2009).

19. Marquez G, Wang LV, Lin SP, Schwartz JA, and Thomsen SL, Appl. Opt 37, 798 (1998). [PubMed: 18268655]

20. ASHRAE, ASHRAE Handbook–Fundamentals (American Society of Heating, Refrigerating and Air-Conditioning Engineers, 1989), Vol. 1.
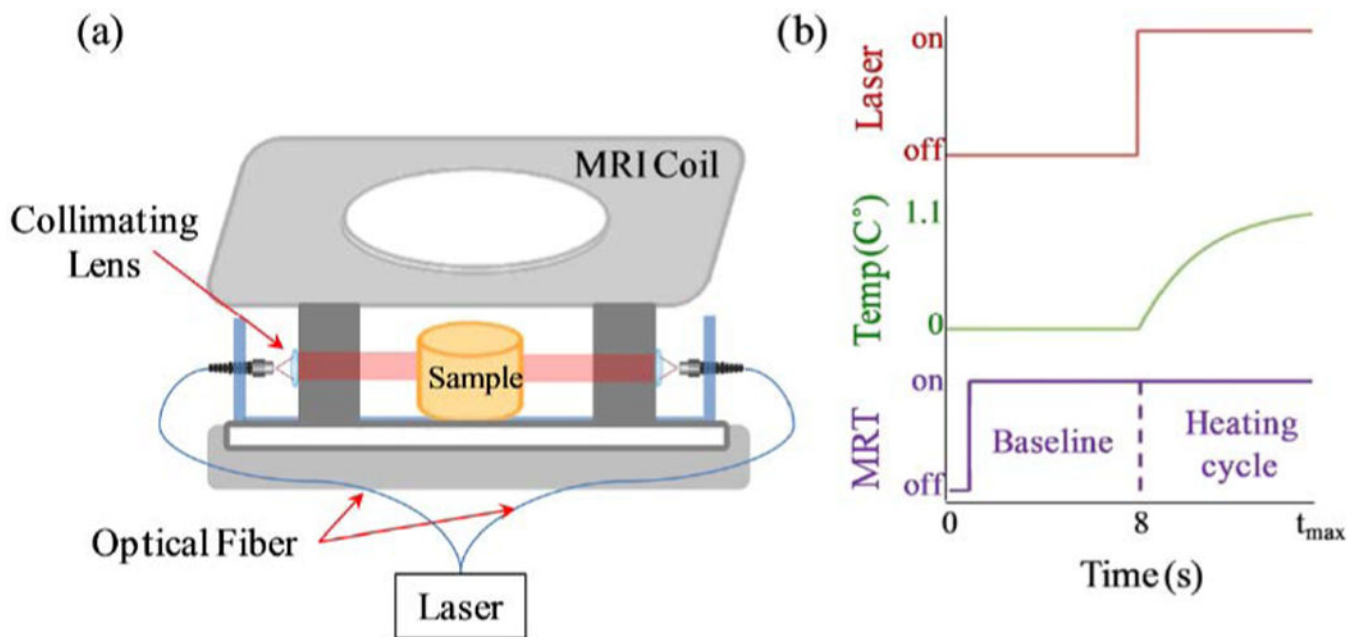
**Fig. 1.**
(a) Schematic of the PMI breast imaging interface: the sample is placed at the center of the coil and illuminated from both sides. The light is transferred to the interface using optical fibers and collimated using aspherical lenses. (b) The PMI data acquisition timeline: the temporal resolution of the dynamic MRT sequence is 8 s. The laser is turned on after the acquisition of the first MRT baseline image, and phase images are acquired during this heating-phase as the temperature of the medium rises.
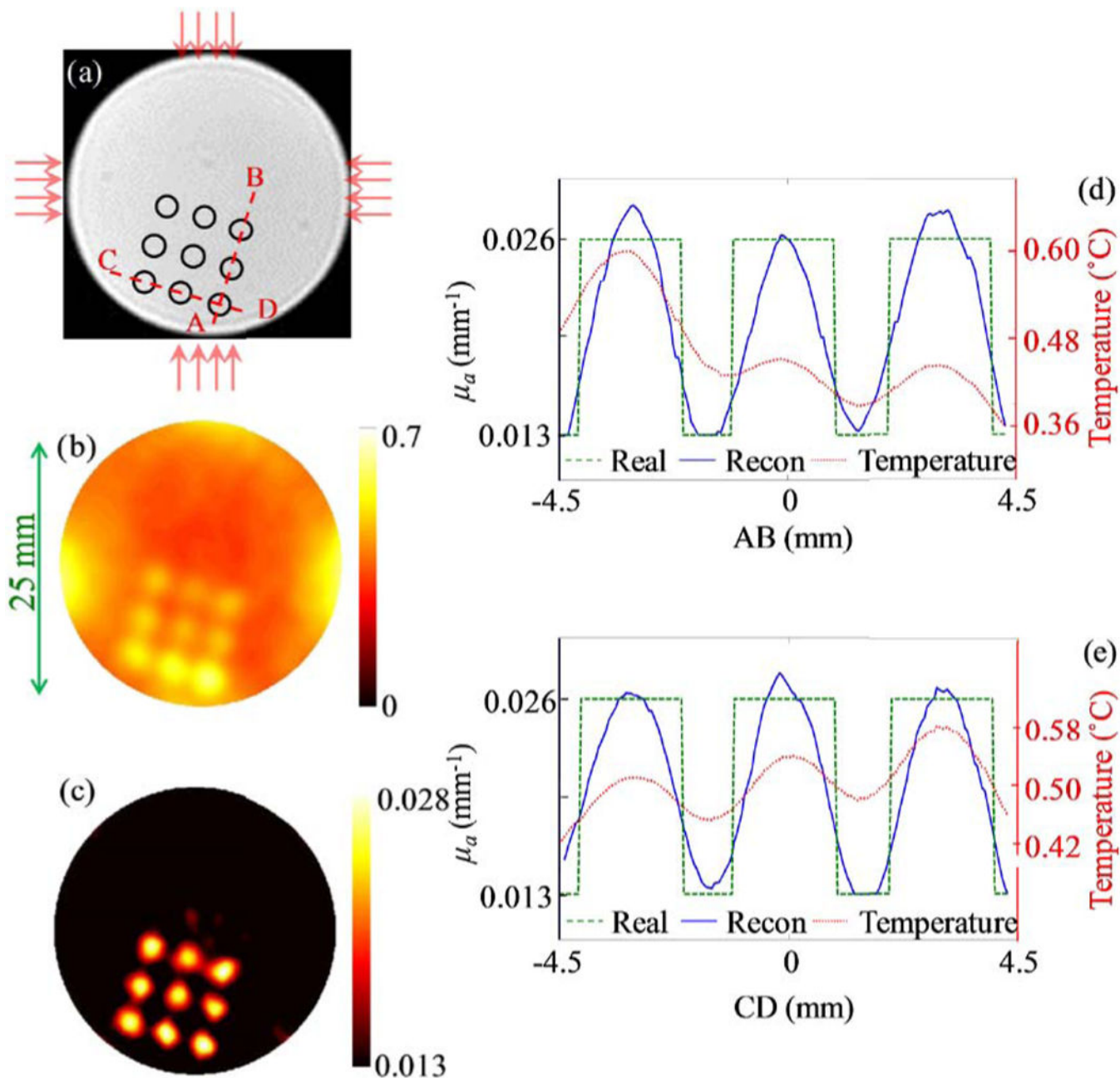
**Fig. 2.**
(a) T1-weighted MR cross section of the phantom. The position of the inclusions is indicated with black circles due to the absence of contrast in the MR image. The illumination spots are indicated by red arrows. (b) The measured temperature increase obtained by MRT at the first frame after 8 s of heating. (c) The reconstructed absorption map using PMI. The profiles performed on both the temperature and absorption maps along (d) line AB and (e) line CD in (a).
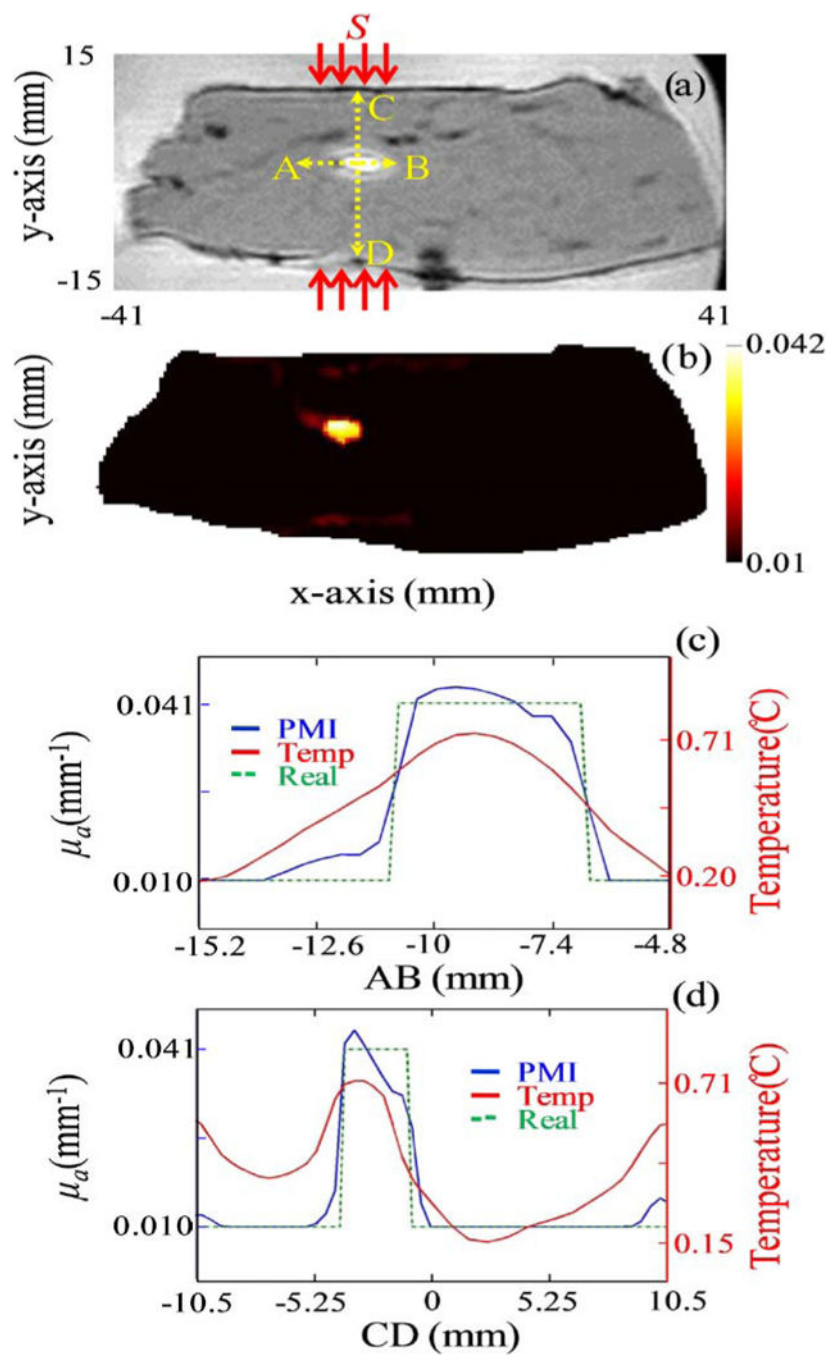
**Fig. 3.**
(a) T1-weighted MR cross section of the chicken breast sample. The illumination spots are indicated by red arrows. (b) The reconstructed absorption map using PMI. The profiles performed on the absorption map along (c) line AB (*x*-axis) and (d) line CD (*y*-axis) in (a).